*The 2019 World Congress on*
***Advances in Structural Engineering and Mechanics (ASEM19)***
*Jeju Island, Korea, September 17 - 21, 2019*

# Analysis of adhesive anchor connection in concrete using nonlinear continuum finite elements

Jafarali Parol [*1], Jamal Al-Qazweeni[2], Shaikha Al-Sanad[3]

[1]*Associate Research Scientist, Kuwait Institute for Scientific Research, Kuwait, Email: jparol@kisr.edu.kw*
[2]*Associate Research Scientist, Kuwait Institute for Scientific Research, Kuwait, Email: jqazweni@kisr.edu.kw*
[3]*Associate Research Scientist, Kuwait Institute for Scientific Research, Kuwait, Email: ssanad@kisr.edu.kw*

*(Received keep as blank , Revised keep as blank , Accepted keep as blank )*

**Abstract.** Crack patterns, failure mechanism and load carrying capacity of adhesive anchor connection in concrete are examined in detail by using nonlinear continuous finite element models. Results of several nonlinear finite element analysis is presented in this paper. The results are compared against experimental results. It is shown here that the finite element model predicts crack patterns and failure mechanisms of adhesive anchor connections quite accurately. Effect of combined tension and shear loads (vertical alignment of anchor) on the breakout capacity is examined. As the shear force component increases, load carrying capacity reduced significantly associated with change in failure mode. Furthermore, cracks patterns were different in the latter case.

**Keywords:** Adhesive anchor, Reinforced concrete, finite element analysis

## 1. Introduction

Anchors are quite commonly used to connect precast concrete structural elements, retrofit concrete structural elements with steel structures, concrete–steel composite structures etc. Anchors used in concrete can be generally classified into two categories, namely, the cast in situ and the post-installed retrofit anchors. Retrofit anchors are used to strengthen exiting damaged structural elements. Strengthening of damaged reinforced concrete structures using steel frames connected to the concrete structural elements using steel anchors is one of the common repair practices. Efficiency of such a retrofit system totally depends on the load transfer between the concrete and steel structural elements through these anchor connections. It was reported that, the anchor connections fail (concrete cone failure or any other damage mechanism) against tensile and shear loads prior to the failure in the existing primary structural system.

Anchors can be further classified based on the load transfer mechanism between the anchors and the base material such as expansion anchors, undercut anchors, and adhesive or grouted anchors. In an expansion anchor system, the load from the anchor to the base material is transferred by friction, and in an undercut anchor system, the applied load is transferred by the mechanical interlock with the base material (ACI 318M-11, 2011; Werner et al, 1995). Adhesive anchors consist of a threaded road bonded with the base material using a chemical epoxy or cement grouting. Adhesive anchors transfer the load to the base material by chemical bonding between the anchor and the base material concrete (Cook *et al*., 1992, 1998).

Behavior of anchor connections between a metal and another metal is quite different from a steel to concrete connection. In a steel–to–concrete anchor connections the failures are determined either by the failure of steel anchor or the brittle failure of concrete. The latter failure mode is unique to steel-concrete anchor connections. These failure modes are affected by many parameters such as alignment of anchors, edge distance, spacing of anchors, diameter of anchors, embedment length of anchors, grade of concrete etc. Most of the theories and design guidelines for anchor connections in RC

* Corresponding author, Ph.D, E-mail: jparol@kisr.edu.kw

structures are derived based on the behavior of a single anchor connection and empirical rules. Many research papers have been reported related to this subject (Cook, 1993; Conard 1969; Mehmet *et al*., 2005).

Cook *et al*. (1998) presented a mathematical model for the design of a single adhesive anchor based on uniform bond stress model. This model was obtained using a best-fit derived from the experimental data. They proposed an optional modification factor for concrete strength. However, their conclusions were based on limited experimental results. Cook *et al*. (1992) showed that the adhesive and grouted anchors with insufficient embedment depth, need not necessarily fail in concrete breakout. Instead, a combination of pullout and concrete breakout failure could be possible. Conard (1969) examined the loading characteristics of several types of grouted anchors. According to him, the best results were obtained using a nonshrink grout. Recently, Salih and co-authors studied the behavior of anchors in low strength concrete (Salih *et al*., 2013; Ozlem *et al*., 2013). Salih *et al*., recommended that embedment depth and free edge distance must be at least 15 times bar diameter to obtain a ductile behavior. They observed a reduction in shear strength due to increase in anchor diameter and with the lower strength concrete.

Comparison of experimental results with commonly used design approaches were presented by several investigators (Mehmet *et al*., 2005; Cook, 1993). Mehmet *et al*., (2005) investigated the behavior of post-installed anchors in plain and fiber reinforced concretes. Cook (1993) provided design recommendations based on rational analysis of the test results and observed failure modes. Higgins *et al*. (1998) published findings on the response of post-installed anchors due to various environmental exposure conditions and they recommended design procedures for environmentally exposed post-installed anchors. Gesoglu et al. (2005) conducted experimental tests on the behavior of post-installed anchors embedded in plain and steel fiber-reinforced normal-strength and high-performance concrete.

The behavior of adhesive anchors was examined using linear and nonlinear finite element analysis by James et al., (1987). Two-dimensional axisymmetric elements were used to model the concrete and anchors. James et al., did not model the relative slip between concrete, epoxy, and anchors. Using the artificial neural network Sherif and Ashraf (2005) showed that the tensile behavior of adhesive anchors was linearly proportional to the embedment depth and concrete compressive strength.

Chang et al., (2011) modelled anchor pullout by incorporating the heterogeneity of concrete by randomly assigning strength and elastic modulus using Weibull distribution. They observed a strong size effect on concrete cone failure. Miroslav and Jan (2012) examined the epoxy concrete interface of adhesive anchors. Experimental and finite element analyses were carried out to examine bond behavior. The contact between the glue and concrete was simulated using contact elements with tangential and normal stiffness. However, their work was limited to simulating only anchor pullout due to failure of epoxy bond. Behavior of post installed adhesive anchors in natural stone was examined using experiments and finite element analysis by Loredana and Renato (2014). They investigated the required minimum embedment depth for chemical anchoring of post-installed threaded rods in different natural stones. They have used theoretical formulations developed for concrete. Dongpo et al (2015, 2016) reported that pullout strength increased marginally by increasing anchor diameter for post installed large-diameter anchors installed in concrete foundations. Dongpo et al. (2015) reported that by increasing the anchor diameter, the failure mode changed from steel bar pullout to a combination of cone failure and concrete annulus failure. Dongpo et al. (2016) proposed a modified design equation for large diameter anchors. Brencich (2015) presented a new post-installed wedge anchor and performed calibration procedure for six classifications of concrete and five different stress distributions. According to him the method is more reliable compared to other traditional wedge anchors. Kränkel et al (2015) described a nonlinear viscoelastic deformation behavior of bonded anchors under sustained load. In their mathematical, model the material degradation, applied stress level and the duration of the applied load were included.
Miroslav and Jan (2012) conducted experimental studies and numerical analyses to understand the glue–concrete interface of bonded anchors subjected to tensile load using commonly used industrial glues. They presented a relation describing the load and bearing capacity of bonded anchors subjected to tensile load for the combined concrete-glue failure mode. Jin-Sup et al (2013) successfully employed a 3D finite element model for the anchor systems using ABAQUS to validate the experimental results.

In this paper, continuous nonlinear finite element analysis is employed for the analysis of adhesive anchor connection in concrete. Detailed parametric study was performed to study the effect of vertical alignment of the anchor and edge distance. Effect of vertical alignment can be examined by

studying the effect combined application of tensile and shear load on a vertically aligned anchor. In both cases, The anchor will be subjected to axial tensile load and a shear load component. It is observed that in such case, failure mechanism changed from the concrete cone damage to combined pull out-concrete cone damage as the shear load component (or the inclination of the anchor) increased. Furthermore, as the minimum distance from the concrete edge to the anchor decreased, the load carrying capacity of the connection system decreased significantly.

## 2. Finite Element Constitutive Material Models

Crack modeling in concrete can be categorized into discrete and smeared crack approaches. In the discrete approach, crack is modelled as a geometric discontinuity by disconnecting the cracked elements along its edges. On the other hand, smeared crack model originally proposed by Rashid (1968) assumes the cracked solid to be a continuum. In this study, the constitutive model based on total strain rotating smeared crack model was employed. The constitutive model for the total strain based on the modified compression field theory was originally proposed by Vecchio and Collins (1993). The three-dimensional extension to this theory proposed by Selby & Vecchio (1993) was employed in the present work.

In the smeared crack model, the total strain is decomposed into elastic strain and cracked strain.

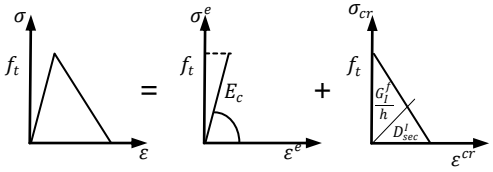


**Fig. 1.** Tension behavior of concrete with linear tension softening.

The total strain decomposed into elastic strain and cracked strain (Fig.1) can be expressed as

$$\varepsilon = \varepsilon^e + \varepsilon^{cr} \quad (1)$$

Where, $\varepsilon$ is the total strain, the elastic strain, $\varepsilon^e = E_c \sigma_c$ (for an equivalent uniaxial case) and $\varepsilon^{cr}$ is the cracked (or plastic) strain. Here, $E_c$, is the Young's modulus of the concrete, and $\sigma_c$ is the elastic stress in concrete (linear portion of the stress strain relation, Fig. 1).

The strain vector in Equation 8 is in the global coordinate system and for a three-dimensional solid model, they have six components and can be expressed as the following:

$$\{\varepsilon^{cr}\} = \left[\varepsilon_{xx}^{cr}\ \varepsilon_{yy}^{cr}\ \varepsilon_{zz}^{cr}\ \gamma_{xy}^{cr}\ \gamma_{yz}^{cr}\ \gamma_{xz}^{cr}\right]^T \quad (2)$$

where *x*, *y* and *z* refer to the global coordinate axes and superscript *T* denotes a transpose. In the rotating crack model, the crack directions continuously rotates with the principal directions of the strain vector, and principal stress and principal strain are coaxial. Hence, no shear strain occurs on the crack plane.

In this study, the linear tension cut off criterion was used for the crack initiation (DIANA, 2018). In other words, when the principal tensile stress exceeds the tensile strength of concrete, a new crack is developed. The coupling effects of different cracks are neglected and for an individual crack and all the crack stresses are solely governed by the corresponding crack, and the constitutive relationship for a given crack is given by

$$\sigma_{nn}^{cr} = D_{sec}^I\ \varepsilon_{nn}^{cr} \quad (3)$$

Here, $\sigma_{nn}^{cr}$ is the cracked normal strain in the local coordinate system. Mode-I secant modulus $D_{sec}^I$ is obtained from the softening relationship between the corresponding stress strain according to,

$$D_{sec,current}^I = min\left[D_{sec,previous}^I\ ,\ \frac{f_{nn}(\varepsilon_{nn}^{cr})}{\varepsilon_{nn}^{cr}}\right] \quad (4)$$

where $\sigma_{nn}^{cr} = f_{nn}(\varepsilon_{nn}^{cr})$ is a general softening relationship of the normal crack stress and normal crack strain. The relationship in general can also be expressed as given below

$$\sigma_{nn}^{cr}(\varepsilon_{nn}^{cr}) = f_t\ y\left(\frac{\varepsilon_{nn}^{cr}}{\varepsilon_{nn,ult}^{cr}}\right) \quad (5)$$

where $f_t$ is the tensile strength, $\varepsilon_{nn,ult}^{cr}$ is the ultimate crack strain. The function $y\left(\frac{\varepsilon_{nn}^{cr}}{\varepsilon_{nn,ult}^{cr}}\right)$ is the function that describes the softening relationship. The softening relationship can be expressed to the Mode-I fracture energy $G_f^I$ through crack band width or element equivalent length *h,* as given below

$$G_f^I = h \int_{\varepsilon_{nn}^{cr}=0}^{\varepsilon_{nn}^{cr}=\propto} \sigma_{nn}^{cr}(\varepsilon_{nn}^{cr})\, d\varepsilon_{nn}^{cr} \quad (6)$$

The ultimate crack strain could be expressed in terms of fracture energy as

$$\varepsilon_{nn,ult}^{cr} = \frac{1}{\alpha}\frac{G_f^I}{hf_t} \quad (7)$$

Here, the value of $\alpha$ is given by

$$\int_{x=0}^{x=\propto} y(x)dx \quad (8)$$

where y(x) is the stress- stress relationship. The ultimate crack strain is inversely proportional to the finite element mesh size and tensile strength and is directly proportional to the fracture energy. In this investigation, linear tension softening was used as shown in Fig. 2. The cracked stress-strain relationship is thus obtained as

$$\frac{\sigma_{nn}^{cr}(\varepsilon_{nn}^{cr})}{f_t} = \begin{Bmatrix} 1 - \frac{\varepsilon_{nn}^{cr}}{\varepsilon_{nn,ult}^{cr}} & if\ 0 < \varepsilon_{nn}^{cr} < \varepsilon_{nn,ult}^{cr} \\ 0 & if\ \varepsilon_{nn,ult}^{cr} < \varepsilon_{nn}^{cr} < \infty \end{Bmatrix} \quad (9)$$

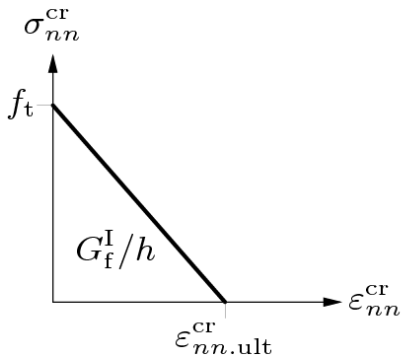


**Fig. 2.** Linear tension softening relationship for concrete.

Substituting Equation 9 into Equation 7, the ultimate crack strain can be expressed as

$$\varepsilon_{nn,ult}^{cr} = 2\frac{G_f^I}{hf_t} \quad (10)$$

Here, $y(x) = (1 - x)$ (Fig.2). The reduced tensile strength can thus be obtained as,

$$f_t = \sqrt{2\frac{G_f^I E_c}{h}} \quad (11)$$

In this study, the crack band width is defined as, $h = \sqrt[3]{V}$, where *V* is the volume of the solid element. It is worth mentioning that $\varepsilon_{nn,ult}^{cr}$ is assumed as a constant in the analysis and is dependent on the element size *h* and material properties such as tensile strength and fracture energy.

## 2.1. *Compression Behavior of Concrete*

The stress strain relationship of concrete in this project was modelled using Thorenfeldt (1987) curve as depicted in Fig. 3.

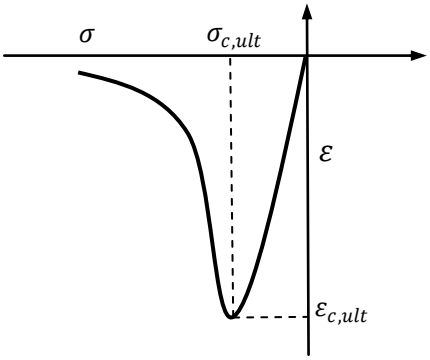


**Fig. 3.** Compression behavior of concrete.

The strength and ductility increase with the increase in isotropic stress and decrease with lateral cracking. These effects were incorporated while obtaining the failure function for compression. If the material was cracked in the lateral direction, the allowable peak stress and peak strain were reduced with a reduction factor (DIANA, 2018).

### *2.2. Bond Slip Behavior*

Bond slip model proposed by Dörr (1980) was used to model the interface between the epoxy and concrete. A cubic polynomial function between the shear traction, $T_t$ and the relative slip *du* between concrete and epoxy contact interface is given by.

$$T_t = \begin{Bmatrix} f_t\left(5\frac{du}{du^0} - 4.5\left(\frac{du}{du^0}\right)^2 + 5\left(\frac{du}{du^0}\right)^3\right) & if\ 0 < du < du^0 \\ 1.9f_t & if\ du > du^0 \end{Bmatrix} \quad (12)$$

where $du^0$ is the maximum allowable relative slip between the epoxy and concrete, above which the traction between the epoxy and concrete remains constant (Equation 12). Graphical representation of variation of the traction and relative slip in the bond slip model is presented in the Fig. 4.

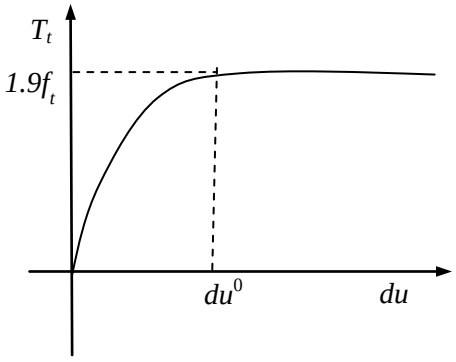


**Fig. 4.** Cubic bond slip behavior between epoxy and concrete.

### *2.3. Steel Anchor and Epoxy Behavior*

The epoxy was modelled as linear elastic. The young's modulus of elasticity was taken as 10 MPa and Poison's ratio equal to 0.3. For the steel anchor, von-Mises plasticity with Tresca's yield criterion was employed (DIANA, 2018). The Young's modulus of elasticity and the poisons ratio of the anchor material were taken as 0.21 GPa and 0.3, respectively.

## 3. Benchmarking of Finite Element Model

### *3.1. Brief description of the Laboratory experiment (Mehmet et al., (2005))*

In the present paper, experimental studies carried out by the Mehmet et al., (2005) is used to benchmark the FE model. They have conducted exhaustive laboratory experiments to study the behavior of adhesive and grouted anchor connection in plain and fiber concrete. In their experiments, a concrete testing block of size 2200 x 1300 x 400 mm was used with a concrete grade of C30. The compressive and splitting tensile strength of the concrete slab is presented in Table 1. Experimental set up used in their work is depicted in Fig 5. Threaded anchors installed using the epoxy with tensile strength 15 MPa, compressive strength 75 MPa and modulus of elasticity of 10 GPA (Mehmet et al., 2005) were used.

**Table 1:** Compressive and Tensile Strengths (28 day) of the Concrete Blocks.

| Compressive strength (MPa) | | Tensile strength (MPa) | |
|---|---|---|---|
| Normal strength concrete | High strength concrete | Normal strength concrete | High strength concrete |
| 30 | 52 | 2.21 | 3.2 |

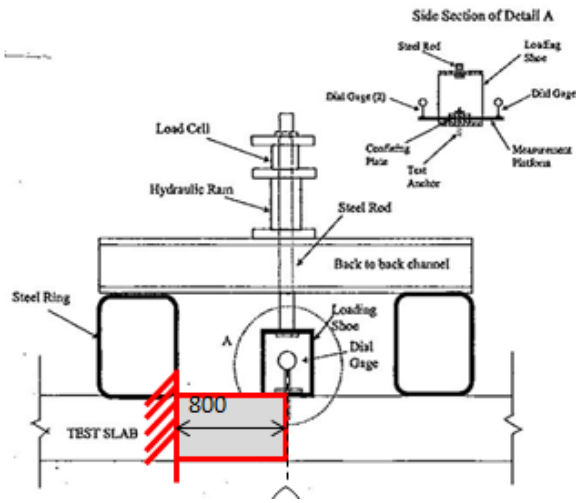


**Fig. 5.** Experimental set up for the laboratory pull out test.

### *3.2. Finite element model for the anchor connection subjected to tensile Load*

Laboratory experiments described in the previous section is with a symmetric geometry, loading and boundary conditions. Hence, only a quarter portion of the concrete-anchor connection to is modelled for the finite element analysis as shown in Fig.6. Eight-nodded 3-D linear brick elements (DIANA, 2018) were used for modelling the concrete slab, anchor and epoxy. For the purpose of bench marking the finite element model, the anchor, epoxy and concrete connections were simulated using the following two approaches in order to choose the right model for the numerical experiments.

#### *3.2.1. Approach 1.*

The connection surfaces between anchor and epoxy, and epoxy and concrete were assumed to be continuous. This is simulated in the finite element model by ensuring nodal connectivity on the interfaces of anchor, epoxy and concrete. This is relatively simpler as it does not allow any relative slip between concrete, epoxy and anchor. This model could be used to simulate the concrete breakout and steel anchor failure modes. However, such a model cannot simulate the anchor pullout failure or

combination of anchor pullout with any other failure modes as it is assumed perfect bond between anchor and epoxy, and concrete and epoxy.

### *3.2.2. Approach 2.*

In this model, the epoxy and anchor was allowed to slide relative to concrete contact surface. This is simulated by modelling the connection surfaces between the epoxy and concrete using bond slip method (Equation 12). For this purpose, interface 2D contact elements were generated at the contact interface of epoxy and concrete. This approach is more general, and can simulate all possible failure modes in adhesive anchor concrete connection. However, this model is computationally expensive and challenging as relative slip occurs at the interface of the epoxy and concrete surface. The background theory of the bond slip model is briefly described in the previous section. Nodes of the bottom face of the anchor in not connected to the concrete and is free in all directions.

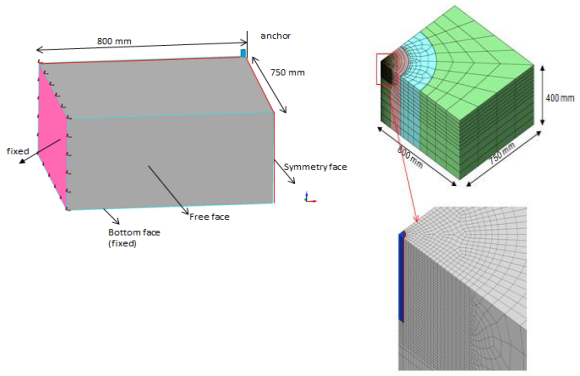


**Fig 6:** Finite element model of the anchor connected to concrete slab.

## 4. Finite element mesh description

The finite element mesh for the anchor, epoxy and concrete connection system is presented in Fig. 6. In both approaches described above, the concrete, steel anchor and the epoxy are modelled as 8 nodded solid brick elements. In the first approach, the epoxy boundary nodes and the concrete are connected and continuous. In the second approach, the boundary nodes of the epoxy and the concrete are not continuously connected. However, the contact face between the epoxy and concrete is modelled using 2D interface elements and the concrete and the epoxy are connected through bond slip relationship as described in Equation (12). This also mean that relative motion of the epoxy and the concrete can be simulated with this.

As described in equation 11, the crack width depends on the finite element mesh size. Hence, the finite element mesh is an important parameter in the nonlinear analysis of such a system. In both approaches, mesh size was carefully chosen (after several trial simulations) and a finite element edge size of 2.5 x 2.5 x 2.5 mm was used for the anchor, epoxy and concrete near the expected cone failure zone. Coarse mesh with the larger element size was used for the concrete slab away from the expected cone failure zone. This particular mesh distribution was chosen to optimize the computational time and memory storage of the results data, at the same time, without compromising on the accuracy of the predicted results.

### *4.2. Loads and Boundary Conditions*

In both cases, (Approach 1 and Approach 2) of finite element models, all of the degrees of freedom at the bottom face and at the far end face (at the edge of the steel ring in the test setup) of the test concrete slab was constrained to zero. On the two symmetric faces, displacements along the normal directions of each surfaces were fixed to zero in order to simulate the symmetry conditions.

Prescribed initial displacement was applied on all the nodes at the top surface of the anchor. It is worth noting that all of these nodes have the same displacement. The displacement was increased by small steps of 0.01mm until failure of the connection system.

## 5. Analysis and Results

### *5.1. Approach - 1*

For the purpose of benchmarking the finite element model, an anchor of 12 mm diameter and 80 mm embedment depth was modelled. In the first approach, as mentioned earlier, the anchor, epoxy, and concrete interfaces were not allowed to displace relative to each other. Young's modulus of elasticity of concrete was taken as 10 MPa and the steel anchor was modelled with linear elastic. The load displacement curve obtained from the finite element analysis is presented in Fig. 7. The finite element model predicted the ultimate failure load of 47.6 kN with concrete breakout failure against the experimental concrete breakout failure load of 46 kN. This is a fairly good match between the finite element model and the experimental result. Concrete breakout occurred along the predicted maximum crack width as depicted in Fig. 9. This predicted cone is approximately at an angle of $45^{o}$ with respect to the anchor. The initial crack was developed near the bottom of the anchor when the displacement reached 0.32 mm. When the displacement reached 0.69 mm the failure cone was fully developed and the connection system failed at 47.6 kN. Additional cracks were developed on top of the concrete due to concrete crushing. The finite element model predicted the stiffness of the anchor connections quite accurately as shown in the load displacement plot (comparing the slope of the load-displacement curves). The displacement distribution at various load steps are shown in Fig. 10. As expected, the portion of concrete away from the breakout cone was not affected during the concrete breakout failure and the displacement in this region was very small compared to the displacement inside of the cone failure zone.

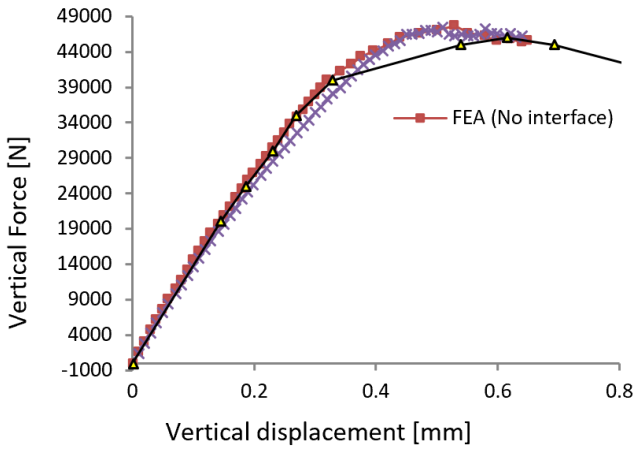


**Fig. 7.** Load displacement curve for the finite element benchmarking model.

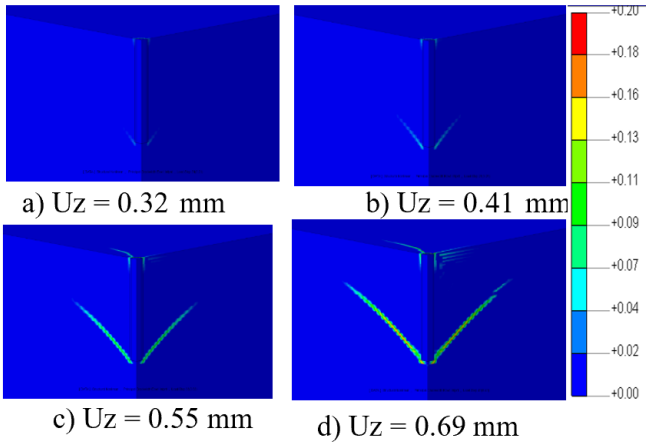


**Fig. 8.** Crack propagation and cone developed at failure load for the anchor connection (Approach 1).

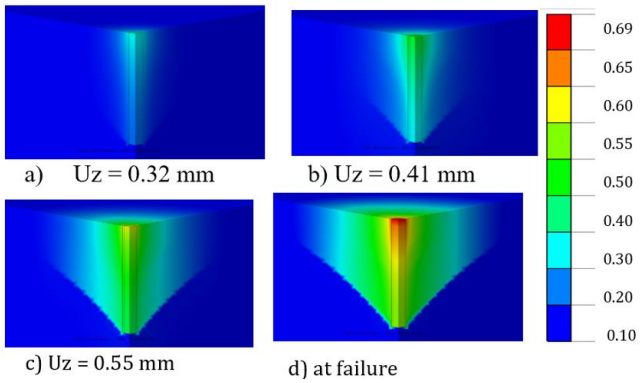


**Fig. 9.** Vertical displacement distribution at various load steps (Approach 1).

### *5.2. FE model with bond-slip contact elements*

In this section, results for the anchor connection system modelled using Approach 2 is described. In this approach, the interface between epoxy and concrete is modelled using the bond slip method. Load displacement curve obtained for various values of bond slip relationship is presented Fig. 12. By suitably choosing the parameters *c* and *du*, one can benchmark various failure modes of an anchor concrete connection system such as concrete breakout failure, anchor pullout, combined breakout and anchor pullout and anchor failure. As an example, with *c* = 8 and *du* = 0.4, the finite element model predicted the concrete breakout failure at 47 kN. This value is close to the experimental result. This model more general where it can simulate all possible failure modes such as the anchor pullout, concrete breakout, steel yielding or a combination of all the three. It is observed that the bond slip model is able to predict the failure mode, stiffness and the of the anchor connections quite well compared with the experiment. In all the following sections for the numerical experiments, we have used the bond slip model.

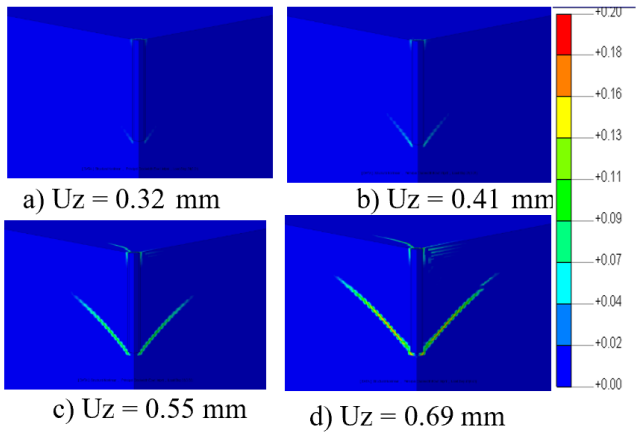


**Fig. 10.** Crack propagation and cone developed at failure load for the anchor connection (Approach 2)

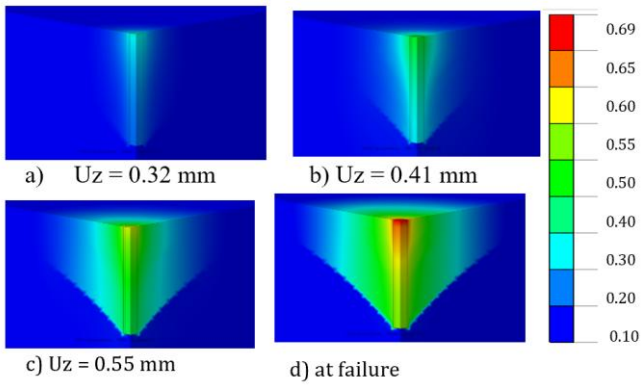


**Fig. 11.** Vertical displacement distribution at various load steps (Approach 2).

## 6. Anchor Subjected to Combined Shear and Tensile Load

Behavior of anchor connection in concrete subjected to both tension and shear simultaneously is examined here. This problem is not a quarter symmetric, but half symmetric. In other words, in this case, half model of the concrete and the anchor connection system is required to be modelled for the analysis. Half symmetric finite element model for a 12 mm diameter anchor with 80 mm embedment depth is shown in the Fig. 10. Load displacement curve is presented in Fig. 11. Tensile load to shear load ratio is varied between 0.18 to 0.27. Failure load in breakout capacity is reduced due to combined load action, and reduction is not very significant for a certain range. Clearly when a threshold value is reached for the ratio, failure load is reduced significantly associated with a change in failure mode. It is observed that as shear component increases, tensile force is developed normal to contact surface of the epoxy and concrete. This reduces the bond strength between the two and opens up the contact surface. Hence, the failure mode changed from breakout to combined pullout and breakout failure. This is clear from Fig. 11 that, when the ratio of tensile load to shear load increased from 0.25 to 0.27, the ultimate failure load dropped to 38 kN associated with a change in change in failure mode. For the ratio = 0.25, the connection failed at concrete breakout and when the ratio was 0.27, the connection failed in pullout failure mode. Crack propagation for the tensile load to shear load ratio = 0.21 and is depicted in Fig. 12. Displacement distribution is presented in Fig. 13.

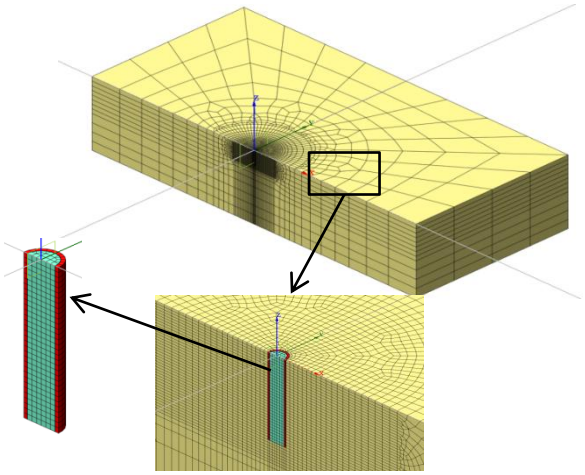

**Fig. 12.** Finite element model for the anchor subjected to combined tension and shear

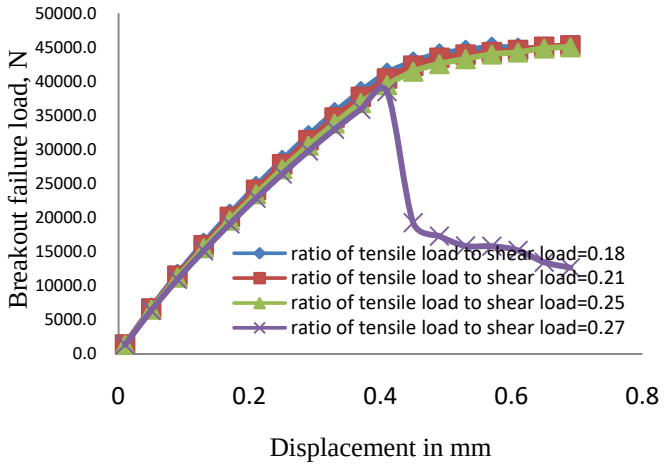


**Fig. 12.** Load displacement curve with combined shear and tension load for 12 mm diameter anchor.

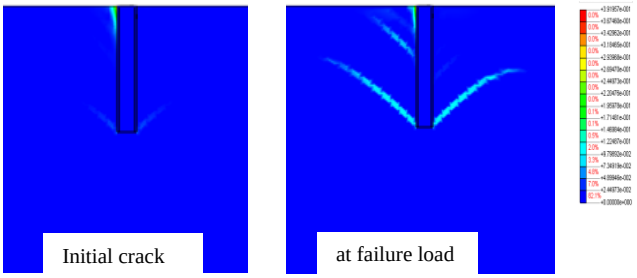


**Fig. 12.** Crack propagation for shear to tension load ratio = 0.21.

In the combine load action, the initial crack is developed from the bottom of the anchor. And the crack is propagated as a cone towards the concrete top surface at 45 degree angle. However, at approximately mid height of the anchor an additional inclined crack parallel to the initial crack is developed only on the tension side of the epoxy concrete bonding (Fig 15). Such an unsymmetrical crack was not present in the case of the anchor subjected to tension load only. Additionally, parallel to the bonding surface of epoxy and concrete, a shear crack is developed due to tension generated normal to the epoxy concrete

bonding surface (Fig 15). This crack was generated at the tension side of the epoxy-concrete bonding. As the percentage of shear load increased, the normal tension load increased on the epoxy concrete bonding and this caused the connection system to fail in pullout failure, when shear to tension ratio reached 0.27.

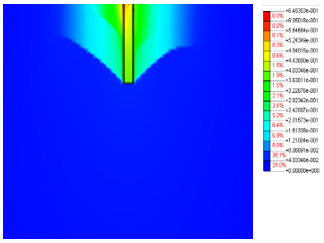

**Fig. 13.** Displacement distribution for shear to tension load ratio = 0.21at failure load.

## 7. Conclusion

Behavior of anchor connection in concrete was examined using continuum nonlinear finite element models. Results were compared against experimental results available in the literature. Important findings and observations from this study are listed below:

- Finite element model is benchmarked against experimental results. The finite element model predicts the experimental results quite accurately.
- When an adhesive anchor connection in concrete subjected to combined tension and shear loads, as the shear component of the applied load increases, failure load of the system reduced significantly. Unsymmetric cracks were generated from the mid height of the anchor depth and also from the top surface of the anchor. Furthermore, the failure mode changed from concrete breakout to combined pullout-concrete breakout failure based on the tensile load to shear load ratio.

## Acknowledgements

The authors would like to thank Kuwait Institute for Scientific Research (KISR) for funding the research work.

## Reference

ACI-318M. 2011. Building code requirements for structural concrete (ACI 318M-11) and commentary. ACI Committee 318, American Concrete Institute, Farmington Hills, MI.

Chang, X.; H. Chen; B. Liu; and F. Zhao. 2011. Modeling of anchor anchor pullout in concrete based on a heterogeneous assumption. *Nuclear Engineering and Design*, **241**, 1345-1351.

Conard, R.F. 1969. Test of grouted anchor anchors in tension and shear. *ACI Structural Journal.* **66(9)**: 465-481.

Cook, R. A. 1993. Behavior of chemically bonded anchors. *Journal of Structural Engineering*. ASCE. **119 (9)**: 2744-2762.

Cook, R. A.; Collins. D. M.; Klinger. R. E., and Polyzois. D. 1992. Load deflection behavior of Cast-in-Place anchors and retrofit anchors. *ACI Structural Journal*. **89(6)**: 639-649.

Cook, R. A.; Kunz, J.; Fuchs. W.; and Konz. R. C.; 1998. Behavior and Design of single adhesive anchors under tensile load in untracked concrete. *ACI Structural Journal*.; **95(1)**: 9-26.

DIANA 10.1, 2018. Reference manual.

Dongpo, W.; Dongsheng W.; Chaojun W. and Mingang Z. 2016. Performance and design of post-installed large diameter anchors in concrete, Construction and Building Materials, 114: 142-150.

Dongpo, W.; Dongsheng W.; Siming H.; Jun Z.; Chaojun O. 2015. Behavior of post-installed large-diameter anchors in concrete foundations, Construction and Building Materials, 95: 124-132.

Dörr, K.; 1980. Ein Beitrag zur Berechnung von Stahlbetonscheiben unter besonderer Berücksichtigung des Verbundverhaltens. PhD thesis, University of Darmstadt.

Gesoglu, M.; T. Özturan,; M. Özel,; and E. Güneyisi. 2005 "Tensile Behavior of Post-Installed Anchors in Plain and Steel Fiber-Reinforced Normal- and High-Strength Concretes," ACI Structural Journal, V. 102, No. 2, pp. 224-231.

Higgins, C. C. and R. E. Klinger. 1998. "Effects of Environmental Exposure on the Performance of Cast-In-Place and Retrofit Anchors in Concrete," ACI Structural Journal, V. 95, No. 5, pp. 506-517.

James, R. W., C. De la Guardia and C. McCreary. R. 1987. Strength of epoxy grouted anchor anchors in concrete. J Struct Divsn ASCE. **113(12)**: 2365-2381.

Loredana, C.; and C. Renato. 2014. Behavior of post-installed adhesive anchors in natural stone. Construction and Building Materials. **68**: 355-369.

Mehmet, G.; O. Turan,; O. Melda, and G. Erhan. 2005. Tensile behavior of post-installed anchors in plain and steel fiber-reinforced normal and high strength concretes. ACI Structural Journal. **102(2)**: 224-231.

Miroslav, B. and B. Jan. 2012. The glue-concrete interface of bonded anchors", Construction and Building Materials. **34**: 267-274.

Ozlem, C.; Y. Salih; K. Hasan; and K. Nevzat, 2013 Shear strength of epoxy anchors embedded into low strength concrete. Construction and Building Materials. **38**: 723-730.

Rashid, Y. R. 1968. Ultimate strength analysis of prestressed concrete pressure vessels Nuclear Engineering and Design, Volume. **7 (4)**: 334–344.

Salih, Y.; A. O. Mohammet and Y. Yavuz. 2013. Tensile behavior of post installed chemical anchors embedded to low strength concrete. Construction and Building Materials. **47**: 861-866.

Selby, R.G.; and Vecchio F. J. 1993. Three-dimensional Constitutive Relations for Reinforced Concrete. Tech. Rep. 93-02, Univ. Toronto, dept. Civil Eng., Toronto, Canada.

Sherif, S. S. S.; and Ashraf F. A. 2005. Prediction of tensile capacity of single adhesive anchors using neural networks. Computers & Structures. **83**: 1792-1803.

Thorenfeldt, E.; A. Tomaszewicz, and J. J. Jensen. 1987. Mechanical properties of high-strength concrete and applications in design. Proceedings of the Symposium. Utilization of High-Strength Concrete (Stavanger, Norway), Tapir.

Vecchio, F. J; and M. P. Collins,. 1993. Compression response of cracked reinforced concrete, J. Str. Eng., ASCE **119 (12)**: 3590-3610.

Werner, F.; E. Rolf and E. B. John. 1995. Concrete capacity design (CCD) approach for fastening to concrete. ACI Structural Journal. **92(1)**: 73-94.